

# Innovative synthesis of mesostructured CoSb<sub>3</sub>-based skutterudites by magnesioréduction

S. Le Tonquesse, E. Alleno, Valérie Demange, V. Dorcet, L. Joanny, C. Prestipino, O. Rouleau, M. Pasturel

► **To cite this version:**

S. Le Tonquesse, E. Alleno, Valérie Demange, V. Dorcet, L. Joanny, et al.. Innovative synthesis of mesostructured CoSb<sub>3</sub>-based skutterudites by magnesioréduction. *Journal of Alloys and Compounds*, Elsevier, 2019, 796, pp.176-184. 10.1016/j.jallcom.2019.04.324 . hal-02161323

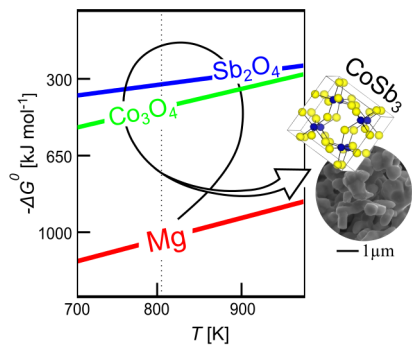
**HAL Id: hal-02161323**

**<https://hal-univ-rennes1.archives-ouvertes.fr/hal-02161323>**

Submitted on 1 Jul 2019

**HAL** is a multi-disciplinary open access archive for the deposit and dissemination of scientific research documents, whether they are published or not. The documents may come from teaching and research institutions in France or abroad, or from public or private research centers.

L'archive ouverte pluridisciplinaire **HAL**, est destinée au dépôt et à la diffusion de documents scientifiques de niveau recherche, publiés ou non, émanant des établissements d'enseignement et de recherche français ou étrangers, des laboratoires publics ou privés.



## Innovative synthesis of mesostructured CoSb<sub>3</sub>-based skutterudites by magnesioreduction

Sylvain Le Tonquesse<sup>a</sup>, Éric Alleno<sup>b</sup>, Valérie Demange<sup>a</sup>, Vincent Dorcet<sup>a</sup>, Loic Joanny<sup>a</sup>, Carmelo Prestipino<sup>a</sup>, Olivier Rouleau<sup>b</sup>, Mathieu Pasturel<sup>a</sup>\*

<sup>a</sup>Univ Rennes, CNRS, ISCR-UMR6226/ScanMAT-UMS2001, F-35000, Rennes, France

<sup>b</sup>Université Paris-Est, Institut de Chimie et des Matériaux Paris-Est, UMR 7182 CNRS - UPEC, 2 rue H. Dunant, 94320 THIAIS, France

---

### Abstract

High purity CoSb<sub>3</sub>, Ni<sub>0.06</sub>Co<sub>0.94</sub>Sb<sub>3</sub> and In<sub>0.13</sub>Co<sub>4</sub>Sb<sub>12</sub> were synthesized from oxides by magnesioreduction. This novel synthesis route to CoSb<sub>3</sub>-based skutterudites directly yields highly crystalline powders with submicronic grain size. Densified mesostructured pellets with an average grain size ranging between 550 and 800 nm were obtained by spark plasma sintering. The strong phonon scattering induced by the mesostructuration leads to a lattice thermal conductivity reduction up to 25 % for CoSb<sub>3</sub> and Ni<sub>0.06</sub>Co<sub>0.94</sub>Sb<sub>3</sub> at 300 K without significantly degrading the electronic properties. Consequently, maximum *ZT* figures-of-merit of 0.09, 0.60 and 0.75 are found for CoSb<sub>3</sub>, Ni<sub>0.06</sub>Co<sub>0.94</sub>Sb<sub>3</sub> and In<sub>0.13</sub>Co<sub>4</sub>Sb<sub>12</sub>, respectively, showing the ability of this scalable process to reach the best performances reported in literature for these compositions at moderate temperature and annealing duration.

**Keywords:** Intermetallics; Thermoelectric materials; Chemical synthesis; Powder metallurgy; Microstructure

---

\*mathieu.pasturel@univ-rennes1.fr

## 1. Introduction

Thermoelectric materials (TM) enable the direct conversion of a temperature gradient into voltage, thus offering the opportunity to directly exchange wasted heat into electricity by highly reliable solid state power generators. However, TM-based technologies are still only used in niche applications because of the low performances, high cost or complex synthesis of the currently available materials [1]. Among them, CoSb<sub>3</sub>-based skutterudites have attracted great attention as promising mid-temperature TM due to their high power factor  $PF = \alpha^2/\rho$  (where  $\alpha$  is the Seebeck coefficient and  $\rho$  the electrical resistivity), good mechanical properties and relatively abundant constituting chemical elements [2, 3, 4, 5]. However its thermal conductivity  $\kappa$  is high - up to  $9 \text{ W m}^{-1} \text{ K}^{-1}$  at 293 K in polycrystalline CoSb<sub>3</sub> [6] - mainly due to the lattice (phonon) contribution  $\kappa_L$  and much less to the charge carrier contribution  $\kappa_e$ , with  $\kappa = \kappa_L + \kappa_e$ .

Any attempt to improve the dimensionless thermoelectric figure-of-merit  $ZT$ , defined as:

$$ZT = \frac{\alpha^2}{\rho(\kappa_L + \kappa_e)} T \quad (1)$$

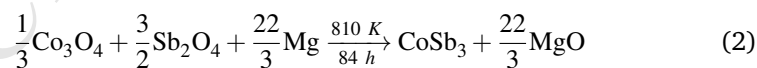
in CoSb<sub>3</sub> involves (i) the optimization of  $PF$  by adjusting the carrier concentration in the semiconducting material and (ii) the reduction of  $\kappa_L$ . The latter can be achieved by creating phonon scattering centers at different length scales in the materials:

(i) At the atomic scale, the most common strategy consists in partially filling the icosahedral  $2a$  crystallographic position of skutterudite structure with heavy atoms. The low energy phonons introduced by the filler atom as well as the mass fluctuation arising from its random occupancy both scatter the heat carrying phonons resulting in a strongly reduced  $\kappa_L$  [7, 8, 9, 10]. Chemical doping on the Co- or Sb-sublattice, which is necessary to achieve optimal charge carrier concentration, has also been shown to affect the thermal conductivity via the mass fluctuation phenomenon [11, 12].

29 (ii) At the microstructural scale, grain boundaries in bulk polycrystalline ma-  
 30 terials also act as effective phonon-scattering centers [13, 14]. Their effect is  
 31 highly intensified in nano- or mesostructured materials where  $\kappa_L$  can be reduced  
 32 by more than 35 % compared to identical materials with much larger grain  
 33 size [15, 16]. As a result, it stimulates the development of alternative synthe-  
 34 sis routes more suitable for the production of submicronic powders than tradi-  
 35 tional melting-annealing methods, such as ball-milling / spark plasma sintering  
 36 (SPS) [17, 18], severe plastic deformation [19], melt spinning [20, 21], com-  
 37 bustion synthesis [22], flash-spark plasma sintering [23], high-pressure synthe-  
 38 ses [24, 25], gas atomization [26] or solution proceed [27, 28]. Improvement  
 39 of  $ZT$  by this approach can only be realized if the decrease of  $\kappa$  is not counter-  
 40 balanced by a decrease of  $PF$  due to overly enhanced electron scattering at the  
 41 grain boundaries.

42 Phonons being more likely scattered by defects with sizes close to their wave-  
 43 lengths, the creation of defects at different length scales in the material, often  
 44 refereed as ‘all-scale hierarchical architectures’, offers the possibility to scat-  
 45 ter phonons over a broader energy spectrum, thus reducing  $\kappa$  more efficiently  
 46 [1, 29, 30, 31]. Very recently, this multi-scale approach have been success-  
 47 fully employed with nanostructured filled-skutterudites [32, 33], porous doped-  
 48 skutterudites [34, 35] or formation of nanoinclusions in filled- and doped-  
 49 skutterudites [36, 37].

50 With this approach in mind, we developed the magnesio-reduction synthesis  
 51 of pristine, Ni-doped and In-filled  $\text{CoSb}_3$  according to the reaction:



52 This new synthesis route to  $\text{CoSb}_3$ -based skutterudites, inspired from indus-  
 53 trial pyrometallurgical processes (*e.g.* Kroll’s process), yields powders with sub-  
 54 micronic grain size that can be readily used for the sintering of mesostructured  
 55 densified materials [38]. It offers other advantages such as the use of air stable  
 56 and cheap oxides as precursors, relatively low temperature and short reaction

57 time compared to conventional melting/annealing synthesis, good control of the  
58 chemical composition and high yield. In this article, the structural, microstruc-  
59 tural and thermoelectric characterizations of these materials are reported and  
60 compared to literature data on similar materials (either mesostructured or not)  
61 prepared by conventional synthesis routes.

## 62 **2. Experimental procedures**

### 63 **2.1. Synthesis of $\text{CoSb}_3$ by magnesioreduction**

64 The first step of the synthesis consists in the preparation of an intimate mixture  
65 of  $\text{Co}_3\text{O}_4$  (Sigma-Aldrich, 99.9 %) and  $\text{Sb}_2\text{O}_4$  (Sigma-Aldrich, 99.995 %) with a  
66 molar ratio of 1:5.4 (20 % excess of  $\text{Sb}_2\text{O}_4$ ) by thoroughly grinding the powders  
67 together in a vibrating mill (Retsch MM200) for 20 min at 25 Hz using tungsten  
68 carbide vial and ball. The oxide mixture was then cold-pressed at 250 MPa into  
69  $\text{Ø}$  10 mm pellets with approximately 2 mm height. Two pellets were stacked  
70 together on top of a Mg chips bed (Strem,  $\geq 99$  %) lying at the bottom of a  
71 Mo crucible (Fig. 1). The quantity of Mg needed to complete the reduction  
72 was determined from the masses of  $\text{Co}_3\text{O}_4$  and  $\text{Sb}_2\text{O}_4$  to be reduced plus an  
73 additional 2-3 % excess. The Mo crucible is then closed and placed in an argon-  
74 filled Inconel tube to prevent its oxidation during the thermal process. The  
75 reactor was heated up to 810 K at  $100 \text{ K h}^{-1}$  and held at this temperature for  
76 84 h before being cooled down to room temperature. After the reaction,  $\text{CoSb}_3$   
77 remains in the shape of compact pellets and could easily be separated from the  
78 loose MgO. The powders were spark plasma sintered (FCT HP-D-10 system) in  
79  $\text{Ø}$  10 mm graphite dies at 910 K and 66 MPa for 5 min with heating/cooling  
80 ramps of  $100 \text{ K min}^{-1}$ .

### 81 **2.2. Synthesis of $\text{Ni}_{0.06}\text{Co}_{0.94}\text{Sb}_3$ and $\text{In}_{0.13}\text{Co}_4\text{Sb}_{12}$ by magne- 82 **sioreduction****

83 The synthesis of Ni-doped and In-inserted  $\text{CoSb}_3$  was attempted from a mixture  
84 of cobalt, nickel/indium and antimony oxides. Nevertheless, the primary for-

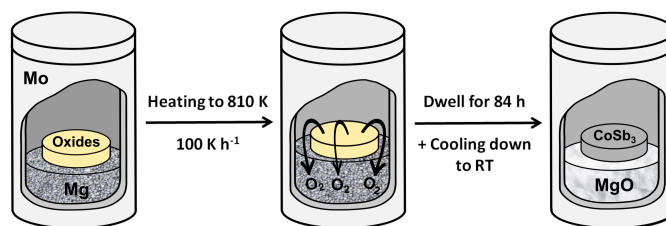


Fig. 1: Experimental procedure for the synthesis of CoSb<sub>3</sub>-based skutterudites by magnesio-reduction of the corresponding (un-)doped Co<sub>3</sub>O<sub>4</sub> and Sb<sub>2</sub>O<sub>4</sub> oxide precursors (yellow pellet). See text for details.

85 mation of NiSb<sub>2</sub> and InSb during the magnesio-reduction process did not allow  
 86 to obtain pure samples in relatively fast and low temperature conditions. Mixed  
 87 precursor oxides were thus prepared in order to start from an intimate mixture  
 88 of metallic ions to speed up the process.

89 For the preparation of Ni<sub>0.18</sub>Co<sub>2.82</sub>O<sub>4</sub> precursor, Co(NO<sub>3</sub>)<sub>2</sub>·6H<sub>2</sub>O (Fluka, ≥  
 90 98%) and Ni(NO<sub>3</sub>)<sub>2</sub>·6H<sub>2</sub>O (Fluka, ≥ 99%) were dissolved in distilled water  
 91 with a molar ratio of about 16:1. The solution was stirred for 30 min and  
 92 evaporated at 363 K. The slurry was ground before being decomposed in air at  
 93 573 K for 4 h leading to the formation of a black powder. The Bragg peaks of  
 94 the X-ray diffraction (XRD) patterns correspond to the Co<sub>3</sub>O<sub>4</sub> structure (*Fd* $\bar{3}m$ )  
 95 with lattice parameter  $a = 8.0905(5) \text{ \AA}$  (Fig. SI.1), suggesting the insertion  
 96 of Ni in Co<sub>3</sub>O<sub>4</sub> ( $a \approx 8.086 \text{ \AA}$ ). Accordingly, the metal ratio determined by X-ray  
 97 energy dispersive spectroscopy (EDS) is in good agreement with the expected  
 98 Ni<sub>0.18</sub>Co<sub>2.82</sub>O<sub>4</sub> composition.

99 For the preparation of In<sub>0.10</sub>Co<sub>2.90</sub>O<sub>4</sub> precursor, CoCl<sub>2</sub>·6H<sub>2</sub>O (Prolabo, 99.9 %)  
 100 and In(NO<sub>3</sub>)<sub>3</sub>·xH<sub>2</sub>O (home made by dissolving metallic indium in concentrated  
 101 nitric acid) were dissolved in distilled water with a molar ratio of about 29:1  
 102 under vigorous stirring. Then a suitable amount (+20 % excess) of NaOH was  
 103 added to form the metal hydroxides. The blue precipitate was then centrifuged,  
 104 washed with water and ethanol, dried overnight at about 363 K and calcinated  
 105 at 723 K to obtain the corresponding oxide. Powder XRD pattern (Fig. SI.2)  
 106 shows broad diffraction peaks corresponding to the Co<sub>3</sub>O<sub>4</sub> structure. Le Bail

107 refinement of the experimental pattern nevertheless converges to a cell param-  
108 eter  $a = 8.102(7) \text{ \AA}$  which could indicate the insertion of In on the Co-lattice  
109 in agreement with recent results by Ma *et al.* [39].

110 From these  $\text{Ni}_{0.18}\text{Co}_{2.82}\text{O}_4$  and  $\text{In}_{0.10}\text{Co}_{2.90}\text{O}_4$  precursors,  $\text{Ni}_{0.06}\text{Co}_{0.94}\text{Sb}_3$  and  
111  $\text{In}_{0.13}\text{Co}_4\text{Sb}_{12}$  were synthesized using the same procedure as for  $\text{CoSb}_3$ , at iden-  
112 tical temperature and duration.

113 These compositions have been selected as (i) the optimized carrier concen-  
114 tration for Ni-doped sample [40, 41] and as (ii) a composition close to those  
115 usually presented in articles dealing with In-inserted skutterudites [42, 43, 44,  
116 45, 46, 47].

### 117 **2.3. Materials characterization**

118 The crystal structure and purity of the samples were checked by powder XRD us-  
119 ing a Bruker D8 Advance diffractometer in the Bragg-Brentano geometry work-  
120 ing with a monochromatized  $\text{Cu K}\alpha_1$  radiation ( $\lambda = 1.5406 \text{ \AA}$ ). The diffractome-  
121 ter is equipped with a 1D LynxEye detector with a photon energy discrimina-  
122 tion around 20 % thus reducing the cobalt fluorescence signal. Lattice constants  
123 were determined by Le Bail refinements as implemented in the FullProf Suite  
124 software [48].

125 Scanning electron microscopy (SEM) images, energy dispersive spectroscopy  
126 (EDS) and electron backscattering diffraction (EBSD) were performed using a  
127 JEOL JSM 7100 F microscope equipped with an Oxford EDS SDD X-Max spec-  
128 trometer and an EBSD HKL Advanced Nordlys Nano detector. Preparation of  
129 the powder samples for SEM analyses consisted in a mere deposition on carbon  
130 tape followed by metallization with carbon. As for the densified samples, the  
131 pellets were successively polished with SiC, diamond paste and colloidal silica  
132 and pasted on SEM holders using silver lacquer. Samples for the transmission  
133 electron microscopy were first thinned by dimpling with colloidal silica and then  
134 by Ar ion milling using a Fischione Ion Mill 1010 operating at 4.5 kV and 5 mA.  
135 Transmission electron microscopy (TEM) analyses were performed on a JEOL  
136 2100 LaB<sub>6</sub> instrument operating at 200 kV and equipped with a high resolution



137 Gatan US1000 camera, and an Orius 200D camera.

138 The Seebeck coefficient  $\alpha(T)$  and electrical resistivity  $\rho(T)$  measurements  
 139 were realized using a home made apparatus described elsewhere [49]. Thermal  
 140 diffusivities were measured in argon atmosphere with the laser flash method us-  
 141 ing a Netzsch LFA 457 equipment. The total thermal conductivity  $\kappa$  was deter-  
 142 mined by multiplying the thermal diffusivity, the specific heat calculated from  
 143 the Dulong-Petit law and the experimental density of the samples.

### 144 3. Results and discussion

#### 145 3.1. Structural and microstructural characterization of as-synthesized 146 and SPSed materials

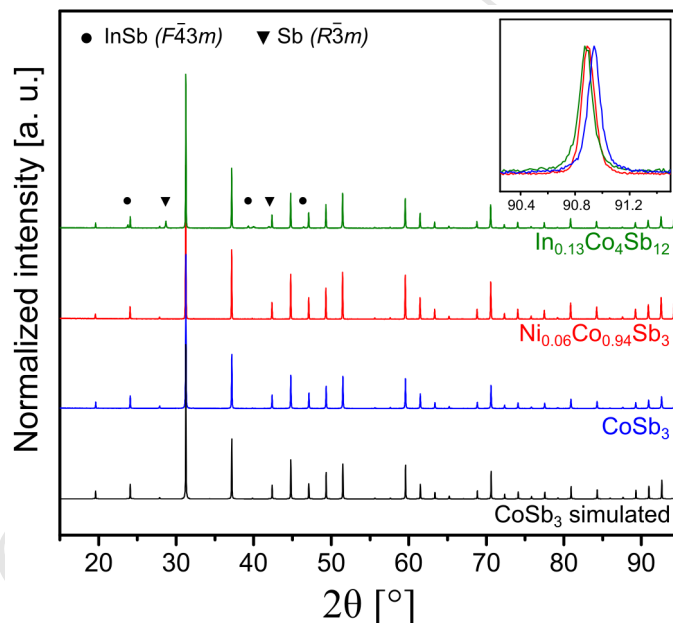


Fig. 2: Experimental XRD patterns of the as-synthesized skutterudite powders and theoretical one calculated with FullProf [48] from cell parameters and atomic positions given in [50] and peak profile function from the utilized diffractometer. The inset shows the shift of the (653) diffraction peak of the  $\text{CoSb}_3$  structure (systematic peak shift due to sample displacement is corrected) revealing the lattice parameter evolution among the samples.

147 The powder XRD patterns of pristine and Ni-doped  $\text{CoSb}_3$  (Fig. 2) are fully

148 indexed according to the skutterudite structure, revealing a single phase prod-  
149 uct. Only few traces of InSb ( $F\bar{4}3m$ ) and Sb ( $R\bar{3}m$ ) are visible on the XRD pattern  
150 of the indium containing compound. Le Bail fitting of the XRD patterns results  
151 in cell parameters of  $a = 9.0350(2)$ ,  $9.0434(1)$  and  $9.0443(6)$  Å for  $\text{CoSb}_3$ ,  
152  $\text{Ni}_{0.06}\text{Co}_{0.94}\text{Sb}_3$  and ' $\text{In}_{0.13}\text{Co}_4\text{Sb}_{12}$ ', respectively, indicating an effective substitu-  
153 tion by nickel on the cobalt site and insertion of indium in the cages of the struc-  
154 ture [44, 51, 52]. By comparison with literature data, one can expect chemical  
155 compositions close to  $\text{Ni}_{0.06}\text{Co}_{0.94}\text{Sb}_3$  and  $\text{In}_{0.10}\text{Co}_4\text{Sb}_{12}$  from these lattice pa-  
156 rameter values [40, 53]. The discrepancy with the targeted In-concentration  
157 could be explained by some residual InSb binary compound in the sample. The  
158 diffraction peaks exhibit very narrow profiles characteristic of well-crystallized  
159 matter which may favor the electrical transport in these materials. Surprisingly,  
160 no traces of MgO are visible on these patterns which is quite unusual for such a  
161 process [54, 55, 56] and may result either from the absence of this by-product  
162 or from its amorphous nature, the reaction being carried out at a relatively low  
163 temperature.

164 SEM examination of the obtained powders reveals faceted submicronic grains  
165 (Fig. 3). The grain size ranges from 300 nm to 1  $\mu\text{m}$  for  $\text{CoSb}_3$  and its Ni-  
166 doped counterpart and from 100 nm to 1  $\mu\text{m}$  for the In-inserted skutterudite.  
167 Such small particles are required to lower the thermal conductivity and are usu-  
168 ally obtained by high energy ball-milling with both risks of contamination from  
169 the milling material and decomposition of the phase. In agreement with the  
170 narrow XRD peaks, the shape of most of the grains clearly indicates their sin-  
171 gle crystalline nature. EDS analyses of the Ni-doped  $\text{CoSb}_3$  powders confirm  
172 the presence of Ni in the sample with a concentration of  $\approx 1$  at.%. On the  
173 other hand, no characteristic X-ray emission peaks of In could be detected for  
174 the filled skutterudite and this could be explained by the low concentration of  
175 the element in the material ( $< 1$  at.%) being below the detection limit of the  
176 technique. No signal of Mg is visible on the X-ray emission spectra from all the  
177 samples.

178 Both XRD and EDS analyses indicate the absence of MgO in the as-synthesized

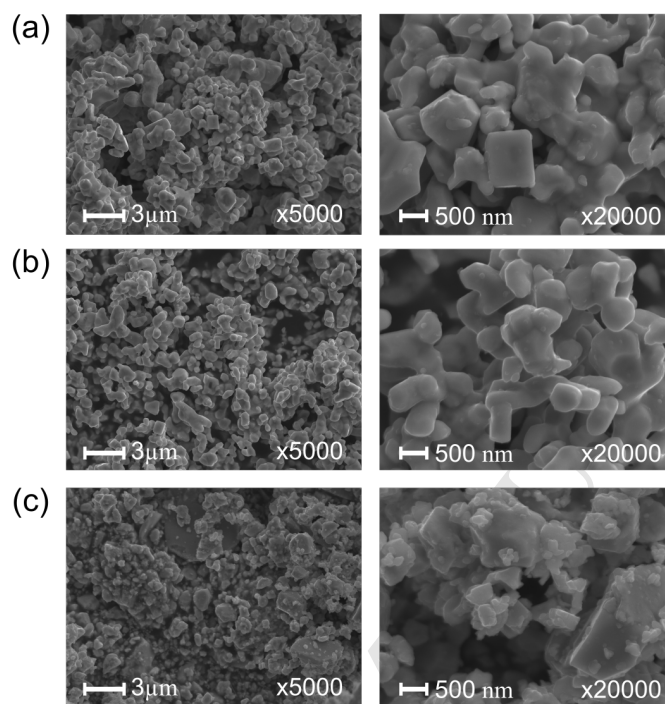


Fig. 3: Secondary electron SEM images of the as-synthesized (a)  $\text{CoSb}_3$  (b)  $\text{Ni}_{0.06}\text{Co}_{0.94}\text{Sb}_3$  and (c)  $\text{In}_{0.13}\text{Co}_4\text{Sb}_{12}$  at two different magnifications.

179 products. In addition, TEM observations coupled with EDS analyses did not  
 180 reveal any traces of Mg or MgO particles in the samples. Together with the re-  
 181 tention of both mixed-oxide pellet and magnesium turning shapes, and based  
 182 on the Ellingham diagram [57] for the metals in presence, we hypothesize  
 183 solid-gas driven reduction reactions at 810 K: Mg consumes the residual  $\text{O}_2$   
 184 atmosphere in the crucible ( $p_{eq}(\text{O}_2) = 10^{-63}$  Pa) inducing the decomposition of  
 185  $\text{Co}_3\text{O}_4$  ( $p_{eq}(\text{O}_2) = 10^{-19}$  Pa) and  $\text{Sb}_2\text{O}_4$  ( $p_{eq}(\text{O}_2) = 10^{-14}$  Pa) into native metals  
 186 that readily react together to form the skutterudite phase.

187 Spark plasma sintering was used to prepare the skutterudite pellets because  
 188 it can achieve high densities in short sintering times thus limiting grain growth  
 189 during the densification process. With the sintering conditions given in 2.1,  
 190 relative densities ranging from 96 to 97 % were obtained (Table 1).

191 Le Bail fitting of the XRD patterns measured on sintered pellets polished

192 surfaces (Fig. 4 and SI.4) do not show significant evolution of the unit cell  
 193 parameter for  $\text{CoSb}_3$  and  $\text{Ni}_{0.06}\text{Co}_{0.94}\text{Sb}_3$  ( $a = 9.0361(2)$  and  $9.0428(1)$  Å,  
 194 respectively). A significant increase up to  $a = 9.0482(3)$  Å is observed for  
 195  $\text{In}_{0.13}\text{Co}_4\text{Sb}_{12}$ , which, together with the disappearance of the InSb Bragg peaks,  
 196 is attributed to a higher insertion of indium in the cages available in the skutterudite  
 197 structure. Considering the low melting point (789 K) reported for InSb  
 198 [58], its reactivity with the skutterudite matrix during the sintering process per-  
 199 formed above this melting point was expected. Only a very small amount of  
 200 antimony ( $R\bar{3}m$ ) could be detected by XRD after sintering and it was found to  
 201 represent less than 1 wt.% of the sample. The latter cell parameter corresponds  
 202 to the composition  $\text{In}_x\text{Co}_4\text{Sb}_{12}$  with  $0.13 \leq x \leq 0.15$ , depending on the literature  
 203 data [42, 53].

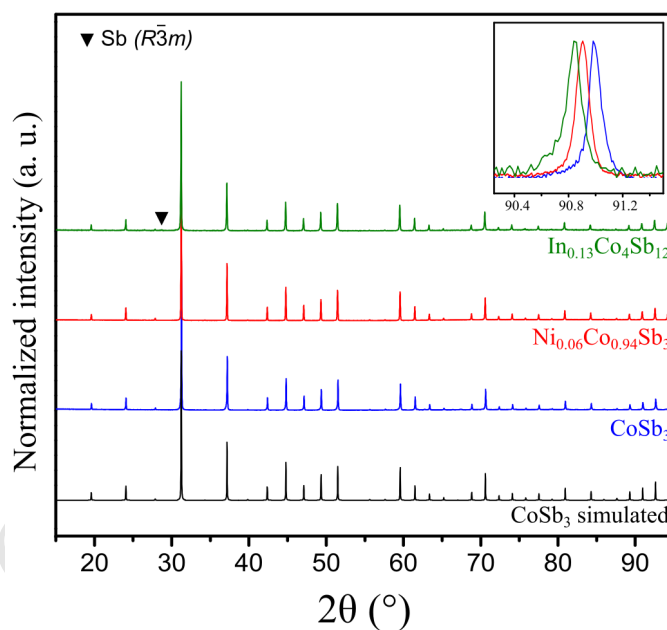


Fig. 4: Experimental XRD patterns of the sintered skutterudite pellets and theoretical one calculated with FullProf [48] from cell parameters and atomic positions given in [50] and peak profile function from the utilized diffractometer. The inset shows the shift of the (653) diffraction peak of the  $\text{CoSb}_3$  structure (systematic peak shift due to sample displacement is corrected) revealing the lattice parameter evolution among the samples.

204 SEM-EDS analyses performed on several spots of the polished surfaces gives

205 a mean Ni concentration of 1.5 at.% for the Ni-doped samples, which is in good  
 206 agreement with the targeted and crystallographic compositions. This composi-  
 207 tion is homogeneous through the analyzed polished surface and no concentra-  
 208 tion gradient is observed. As for the powders, no significant In or Mg content  
 209 could be detected on any samples by EDS analyses which means that those ele-  
 210 ments are in concentration below the detection limit of the technique.

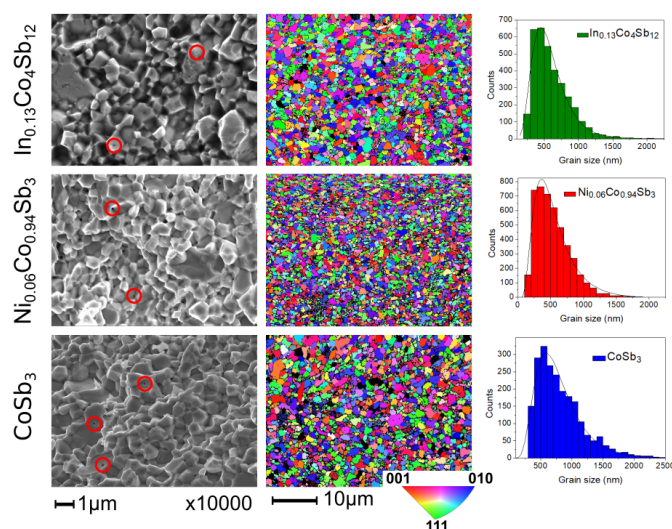


Fig. 5: Secondary electron SEM images of the pellet cross-sections (left) showing some residual porosity (circled in red). EBSD mappings (middle) of the polished pellet surfaces and histograms (right) showing the distribution of grain sizes determined from EBSD maps for the SPSeD  $\text{CoSb}_3$  (bottom),  $\text{Ni}_{0.06}\text{Co}_{0.94}\text{Sb}_3$  (middle) and  $\text{In}_{0.13}\text{Co}_4\text{Sb}_{12}$  (top) skutterudites.

211 In order to check how sintering affects grain size, electron backscattering  
 212 diffraction (EBSD) and SEM imaging (Fig. 5) were performed on polished sur-  
 213 faces and on broken cross-sections of the pellets, respectively. SEM imaging  
 214 reveals some closed porosity (encircled in red) which is responsible for the full  
 215 densification deviation. EBSD mappings were realized on a  $1750.5 \pm 9.5 \mu\text{m}^2$   
 216 area with a step size of 100 nm for  $\text{CoSb}_3$  and  $\text{In}_{0.13}\text{Co}_4\text{Sb}_{12}$  and 50 nm for  
 217  $\text{Ni}_{0.06}\text{Co}_{0.94}\text{Sb}_3$  to distinguish better smaller grains. Kikuchi lines were well in-  
 218 dexed using the skutterudite structure and cell parameters obtained from XRD,  
 219 and only a few non-indexed areas were found on the 3 pellets. First of all, one

220 can notice a random distribution of the grains orientation throughout the ana-  
 221 lyzed areas. Then submicronic particles are found to cover the majority of the  
 222 surface in all cases, with apparent smaller sizes for the Ni-doped antimonide  
 223 compared to the other two compounds.

Table 1: Summary of the main structural and microstructural features of the sintered skutterudite pellets used for the thermoelectric characterizations

| Nominal composition                                   | $a$ [Å]   | Impurity [wt.%] | Average grain size [nm] | Relative density [%] |
|---|-----------|-----------------|-------------------------|----------------------|
| CoSb <sub>3</sub>                                     | 9.0362(4) | None            | 784 ± 376               | 96                   |
| Ni <sub>0.06</sub> Co <sub>0.94</sub> Sb <sub>3</sub> | 9.0428(3) | None            | 580 ± 336               | 97                   |
| In <sub>0.13</sub> Co <sub>4</sub> Sb <sub>12</sub>   | 9.0482(3) | Sb (<1)         | 617 ± 292               | 97                   |

224 In order to quantify these observations, image analyses were performed us-  
 225 ing the *Channel 5* software (HKL Technology) by considering all the diffracting  
 226 domains containing at least 7 pixels (*i.e.*  $\sim 0.07 \mu\text{m}^2$ ) for CoSb<sub>3</sub> and In<sub>0.13</sub>Co<sub>4</sub>Sb<sub>12</sub>  
 227 and at least 14 pixels (*i.e.*  $\sim 0.035 \mu\text{m}^2$ ) for Ni<sub>0.06</sub>Co<sub>0.94</sub>Sb<sub>3</sub>. The particles size  
 228 distribution (diameter of an equivalent circle with equal surface, Fig. 5) clearly  
 229 shows a majority of submicronic particles. This distribution has been fitted us-  
 230 ing a log-normal distribution function:

$$f(x) = \frac{A}{x\sigma\sqrt{2\pi}} \cdot \exp\left(-\frac{[\ln(x) - \mu]^2}{2\sigma^2}\right) \quad (3)$$

231 where  $A$ ,  $\mu$  and  $\sigma$  are the fitting parameters. From  $\mu$  and  $\sigma$  values, the average  
 232 grain size  $D$  and its standard deviation  $SD$  can be calculated using the formulae:

$$D = \exp\left(\mu + \frac{\sigma^2}{2}\right) \quad (4)$$

$$SD = \left[(\exp(\sigma^2) - 1) \cdot \exp(2\mu + \sigma^2)\right]^{\frac{1}{2}} \quad (5)$$

233 The average grain sizes are found to range from 780 nm for CoSb<sub>3</sub> down to  
 234 580 nm for Ni<sub>0.06</sub>Co<sub>0.94</sub>Sb<sub>3</sub> with intermediate values for the In-inserted phase  
 235 (Table 1).

236 Such small grain sizes induce numerous grain boundaries, which along the  
 237 presence of defects due to crystal orientation mismatches might be efficient to

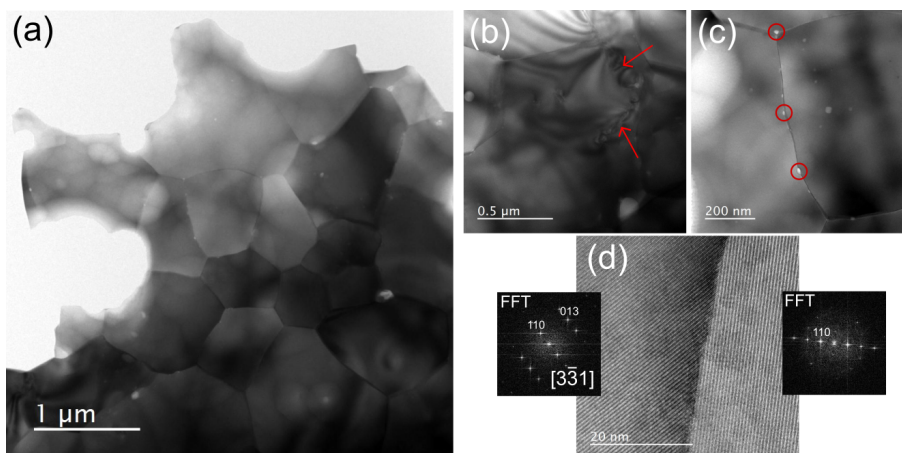


Fig. 6: TEM brightfield images of thinned  $\text{CoSb}_3$  sintered pellet. (a) Typical global area, (b) strips indicating lattice distortions originating from dislocations high density at the grain boundaries (red arrows), (c) nano-scale porosities (encircled in red) and (d) HRTEM image showing the crystallinity of the grain boundaries

238 decrease the lattice thermal conductivity. It was shown that dislocations or  
 239 nanoscale porosity/precipitate can efficiently reduce the skutterudites thermal  
 240 conductivity by phonon scattering [30, 59, 60]. In order to demonstrate the ex-  
 241 istence of such defects in our materials,  $\text{CoSb}_3$  sintered pellet grains boundaries  
 242 have been investigated by TEM. Fig. 6a shows a typical area of the thinned  
 243 pellet where the observations were realized. At this magnification, proper tilt-  
 244 ing of the sample reveals stripes originating from boundaries and propagating  
 245 inside the grains (Fig. 6b). Contrast between those stripes arises from slight  
 246 deviation from the diffraction condition and evidences large lattice constraints  
 247 in the crystal. These are common to sintered materials as they originate from  
 248 high density of dislocations, which are in the present case, mostly located close  
 249 to or at the grain boundaries (red arrows). HRTEM examination of such grain  
 250 boundaries (Fig. 6d and SI.5) reveals that they are well-crystallized and free  
 251 of any amorphous layer. Two major kinds of defects are evidenced in Fig. SI.5  
 252 taken on a semi-coherent lattice interface. Typical dislocations appear inside  
 253 the grains (Fig. SI.5b) while two dimensional analogues of dislocations [61]  
 254 are created at the interface between the grains (Fig. SI.5c), both types being

255 able to scatter mid-wavelength phonons.

256 As shown in Fig. 6c, some porosity with nanometric size (encircled in red)  
257 is also observed at the grain boundaries and can also act as efficient phonon  
258 scattering centers.

259 All these observations are quite common for sintered materials and are not  
260 a special feature resulting from the magnesioreduction synthesis. However, an  
261 exacerbated effect on the thermal conductivity is expected in MR-materials be-  
262 cause of the high grain boundary concentration leading to an elevated defect  
263 concentration.

264

### 265 3.2. Thermoelectric characterizations

266 The electrical resistivities, Seebeck coefficients and thermal conductivities have  
267 been determined in the temperature range 300-800 K where skutterudites usu-  
268 ally present their maximum  $ZT$  value.

269 The electrical resistivity and Seebeck coefficient of the three pellets are  
270 shown in Fig. 7a and 7b.  $\text{CoSb}_3$  shows a semiconducting shape of  $\rho(T)$  in  
271 the 300-800 K temperature range and the  $\alpha(T)$  evolves from strongly nega-  
272 tive at room temperature to positive at 800 K with a sign change at 600 K at-  
273 tributed to the intrinsic regime caused by holes activation through the band gap  
274 [62, 63, 43]. The electrical resistivity of the Ni-doped and In-inserted skutteru-  
275 dites are strongly reduced to respectively 14.5 and 16.0  $\mu\Omega\cdot\text{m}$  at 300 K confirm-  
276 ing the insertion of these elements in the crystal structure. The  $n$ -doping is con-  
277 firmed by the stabilized negative value of  $\alpha(T)$  in both cases, ranging between  
278 -120 and -200  $\mu\text{V K}^{-1}$  for  $\text{Ni}_{0.06}\text{Co}_{0.94}\text{Sb}_3$  and between -180 and -240  $\mu\text{V K}^{-1}$   
279 for  $\text{In}_{0.13}\text{Co}_4\text{Sb}_{12}$  in the investigated temperature range. The electrical resistivi-  
280 ties and Seebeck coefficients are in very good agreement with those reported  
281 for similar compositions of Ni-doped [41, 64] and In-filled [44, 65]  $\text{CoSb}_3$ .  
282 These values lead to an increase of the maximum  $PF$  (Fig. 7c) from about 1  
283  $\text{mW m}^{-1} \text{K}^{-2}$  at 400 K for  $\text{CoSb}_3$  to 3 and 3.5  $\text{mW m}^{-1} \text{K}^{-2}$  for  $\text{Ni}_{0.06}\text{Co}_{0.94}\text{Sb}_3$   
284 at 700 K and  $\text{In}_{0.13}\text{Co}_4\text{Sb}_{12}$  at 600 K, respectively. The small grain sizes and



285 thus a high concentration of grain boundaries do not seem to alter the sample  
 286 transport properties that are dominated by the high crystallinity of the powder  
 287 particles.

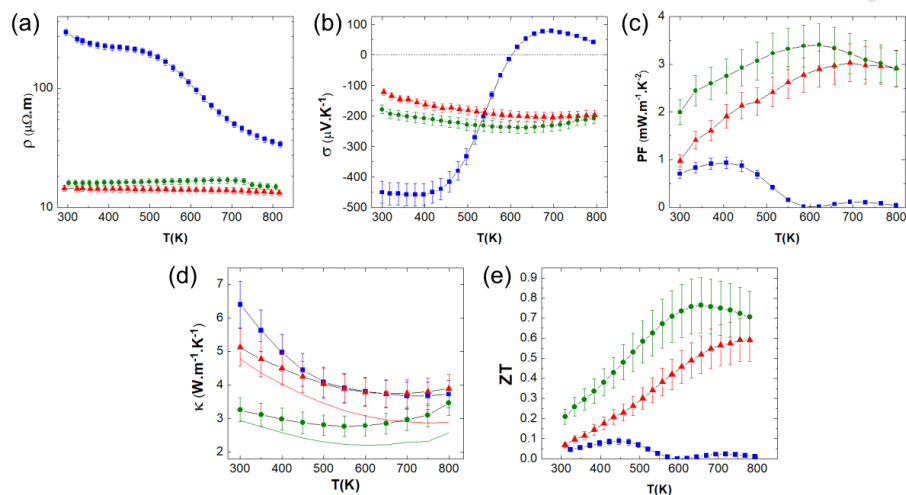


Fig. 7: High-temperature dependence of (a) the electrical resistivity, (b) Seebeck coefficient, (c) power factor, (d) total (symbols) and lattice (solid colored lines) thermal conductivity and (e) figure-of-merit  $ZT$  of (■)  $\text{CoSb}_3$ , (▲)  $\text{Ni}_{0.06}\text{Co}_{0.94}\text{Sb}_3$  and (●)  $\text{In}_{0.13}\text{Co}_4\text{Sb}_{12}$ . Standard deviations have been estimated to 6 %, 8 %, 13 %, 11 % and 18 % for electrical resistivity, Seebeck coefficient, power factor, thermal conductivity and figure-of-merit  $ZT$ , respectively, according to [66]

Table 2: Measured total thermal conductivity and calculated lattice thermal conductivity in  $\text{W m}^{-1} \text{K}^{-1}$  of  $\text{CoSb}_3$ ,  $\text{Ni}_{0.06}\text{Co}_{0.94}\text{Sb}_3$  and  $\text{In}_{0.13}\text{Co}_4\text{Sb}_{12}$  at 300 K and 800 K compared to the thermal conductivities of macrostructured compounds with similar compositions reported in literature.

|   |            | MR samples |       | Literature data     |                     |
|---|------------|------------|-------|---------------------|---------------------|
|   |            | 300 K      | 800 K | 300 K               | 800 K (700 K*)      |
| $\text{CoSb}_3$                               | $\kappa$   | 6.5        | 3.7   | 11.1 [43], 9.2 [44] | 7.5* [43], 4.9 [44] |
|   | $\kappa_L$ | 6.5        | 3.4   | 11.1 [43], 9.0 [44] | 7.2* [43], 4.6 [44] |
| $\text{Ni}_{0.06}\text{Co}_{0.94}\text{Sb}_3$ | $\kappa$   | 5.1        | 3.9   | 6.7 [41]            | 4.4 [41]            |
|   | $\kappa_L$ | 4.7        | 2.9   | 6.3 [41]            | 3.4 [41]            |
| $\text{In}_{0.13}\text{Co}_4\text{Sb}_{12}$   | $\kappa$   | 3.3        | 3.5   | 3.5 [44], 4.6 [65]  | 3.0 [44], 3.2* [65] |
|   | $\kappa_L$ | 2.9        | 2.6   | 3.1 [44], 3.9 [65]  | 2.3 [44], 2.5* [65] |

288

289 The thermal diffusivity of the three synthesized skutterudites has been mea-  
 290 sured on sintered pellets and converted to thermal conductivity (Fig. 7d) using

291 the densities of the pellets and the Dulong and Petit specific heat which usually  
 292 applies for skutterudites in this temperature range. The overall shape of  $\kappa(T)$   
 293 for pristine  $\text{CoSb}_3$  corresponds to that usually reported for this material [44].  
 294 Nevertheless, it ranges from  $6.5 \text{ W m}^{-1} \text{ K}^{-1}$  at 300 K down to  $3.7 \text{ W m}^{-1} \text{ K}^{-1}$  at  
 295 800 K. Values reported for similar materials which were synthesized by conven-  
 296 tional melting-annealing routes and being mostly composed of crystallites much  
 297 larger than  $1 \mu\text{m}$  are between 9-11 down to 5-7.5  $\text{W m}^{-1} \text{ K}^{-1}$  at 300 K and  
 298 700 K, respectively [44, 43, 64]. This corresponds to a reduction of the thermal  
 299 conductivity of at least 25 % on the whole temperature range for the metallo-  
 300 reduced samples. The here presented values are in better agreement with those  
 301 observed for ‘nano’-engineered materials with comparable densities [67, 68].  
 302 A direct correlation can be made between the decrease of the thermal conduc-  
 303 tivity measured for  $\text{CoSb}_3$  and the high concentration of grain boundaries and  
 304 associated defects which were evidenced by EBSD/SEM and TEM analyses and  
 305 act as efficient phonons scattering centers.

306 Because of the larger electronic contribution to the total thermal conduc-  
 307 tivity in the Ni-doped and In-filled samples and to compare more significantly  
 308 with literature data, the lattice thermal conductivities  $\kappa_L$  were calculated by  
 309 subtracting  $\kappa_e$  to  $\kappa_{tot}$  (Table 2 and solid lines in Fig. 7d). The Wiedmann-Franz  
 310 law,  $\kappa_e = LT/\rho$ , was used to obtain  $\kappa_e$  using the measured electrical resistivity  
 311 and a Lorenz number of  $1.6 \times 10^{-8}$  and  $1.7 \times 10^{-8} \text{ W } \Omega \text{ K}^{-2}$  for  $\text{Ni}_{0.06}\text{Co}_{0.94}\text{Sb}_3$   
 312 and  $\text{In}_{0.13}\text{Co}_4\text{Sb}_{12}$ , respectively [41, 44].

313 The total thermal conductivity of  $\text{Ni}_{0.06}\text{Co}_{0.94}\text{Sb}_3$  is 20 % lower than that of  
 314 pristine  $\text{CoSb}_3$  at 300 K and reaches similar values from 450 up to 800 K. This  
 315 reduction of  $\kappa(T)$  at room temperature could be explained (i) by the smaller  
 316 particle size and thus higher density of grain boundaries and associated de-  
 317 fects and (ii) by the higher mass fluctuation on the ‘disordered’ transition metal  
 318 sublattice, both enhancing the scattering of phonons and decreasing  $\kappa_L(T)$ . The  
 319 beneficial effect of the mesostructuration is more apparent when  $\kappa_L$  is compared  
 320 to the values reported for conventionally synthesized macrostructured materi-  
 321 als and where a reduction of  $\approx 25 \%$  is noticed at 300 K (Table 2). At higher

322 temperature, the mesostructuration seems to become less and less efficient so  
323 that at 800 K the reduction of  $\kappa_L$  falls to  $\approx 15\%$ . Again, the measured trend  
324 and values are in good agreement with reported mesostructured samples with  
325 a similar doping level [41, 69].

326 With the insertion of indium rattlers in the structure, the total thermal con-  
327 ductivity of  $\text{In}_{0.13}\text{Co}_4\text{Sb}_{12}$  is further lowered to 3.2 and 3.5  $\text{W m}^{-1} \text{K}^{-1}$  at 300  
328 and 800 K, respectively, with a minimum of 2.8  $\text{W m}^{-1} \text{K}^{-1}$  at about 550 K.  
329 These correspond to  $\kappa_L$  of 2.9  $\text{W m}^{-1} \text{K}^{-1}$  at 300 K and 2.6  $\text{W m}^{-1} \text{K}^{-1}$  at 800 K.  
330 Comparisons with literature data are rather difficult due to the wide span of  
331 (effective) rattler concentration and pellet densities encountered and to the rel-  
332 atively large standard deviations inherent to thermal diffusivity measurements.  
333 However the presently investigated sample seems to have a slightly lower  $\kappa_L$  than  
334 reported value but without strong effect from the mesostructuration opposite to  
335 our observations on the two previous compositions. According to Benyahia *et*  
336 *al.* [70] who investigated the influence of grain size on  $\text{In}_{0.25}\text{Co}_4\text{Sb}_{12}$  lattice  
337 thermal conductivity, the reduction of  $\kappa_L(T)$  by mesostructuration would have  
338 a stronger effect from room temperature to  $\approx 580$  K while at higher tempera-  
339 ture scattering by the rattler would become dominant. This could explain why  
340 magnesio-reduced samples have a low  $\kappa_L$  at 300 K compared to those reported  
341 in literature but is only in the average at 700 K. Furthermore, in the above  
342 mentioned article, a modified Nan and Birringer law [71, 72] was used to es-  
343 timate the reduction of  $\kappa_L$  according to the reciprocal of the crystallite size in  
344  $\text{In}_{0.25}\text{Co}_4\text{Sb}_{12}$  at 300 K. Applying here this law and considering a mean crystallite  
345 size of 600 nm, a reduction of  $\kappa_L(300 \text{ K})$  of only  $\approx 10\%$  is estimated compared  
346 to macrostructured materials. This must be taken as a rough estimate since the  
347 synthesis routes and the methods for grain size determination are different, but  
348 it would support the reduction of  $\kappa_L(T)$  thanks to mesostructuration especially  
349 near room temperature in  $\text{In}_{0.13}\text{Co}_4\text{Sb}_{12}$ .

350 The measured physical properties enable to calculate the figure-of-merit  $ZT$   
351 of these materials (Fig. 7e). The  $ZT$  values of pristine  $\text{CoSb}_3$  are small due to  
352 the combined high electrical resistivity and the occurrence of the bipolar effect

353 around 500 K. The obtained values for the Ni-doped and In-filled  $\text{CoSb}_3$  increase  
354  $ZT$  up to 0.6 at 800 K and 0.75 at 650 K, respectively. In the case of Ni-doped  
355  $\text{CoSb}_3$ , this result is very similar to the improved  $ZT$  reported for mesostructu-  
356 tured  $\text{Ni}_{0.06}\text{Co}_{0.94}\text{Sb}_3$  where the reduction of the grain sizes and consequently of  
357 the thermal conductivities was realized by high energy ball-milling [69, 41]. In  
358 the case of  $\text{In}_{0.13}\text{Co}_4\text{Sb}_{12}$ , the reduction of  $\kappa$  by mesostructuration is less effec-  
359 tive due to the elevated phonon diffusion by In-rattlers and the calculated  $ZT$   
360 corresponds well to materials synthesized by conventional melting/annealing  
361 methods [43, 44, 65].

362

## 363 4. Conclusions

364 Pure, Ni-doped and In-filled  $\text{CoSb}_3$  were synthesized from metal oxides in only  
365 84 h at temperature as low as 810 K by a magnesioreduction process. As-  
366 synthesized powders are directly composed of well-crystallized submicronic par-  
367 ticles. After spark plasma sintering, pellets with excellent purities and high  
368 densities were obtained. XRD and SEM analyses show that the dopant and rat-  
369 tler concentrations are very close to the targetted ones, indicating that a good  
370 control of the chemical composition is possible with this process. After sinter-  
371 ing, the average grain size are found to be 780, 580 and 620 nm for  $\text{CoSb}_3$ ,  
372  $\text{Ni}_{0.06}\text{Co}_{0.94}\text{Sb}_3$  and  $\text{In}_{0.13}\text{Co}_4\text{Sb}_{12}$ , respectively. Such small grain size along with  
373 the presence of crystal defects and nanoporosity at the grain boundaries were  
374 shown to decrease the lattice thermal conductivity of the samples especially for  
375  $\text{CoSb}_3$  and  $\text{Ni}_{0.06}\text{Co}_{0.94}\text{Sb}_3$  where strong  $\kappa_L$  reduction of 25 % were observed at  
376 300 K. The electrical resistivity and Seebeck coefficient measurements show no  
377 degradation of the transport properties due to the reduction of grain sizes. This  
378 synthesis route thus directly leads to materials approaching the ‘phonon glass-  
379 electron crystal’ state [73]. It results in  $ZT_{max}$  of 0.09 at 450 K, 0.60 at 800 K and  
380 0.75 at 650 K for  $\text{CoSb}_3$ ,  $\text{Ni}_{0.06}\text{Co}_{0.94}\text{Sb}_3$  and  $\text{In}_{0.13}\text{Co}_4\text{Sb}_{12}$ , respectively. These  
381 values are close to those reported in literature for similar compositions but af-  
382 ter multistep high temperature syntheses followed by various mesostructura-

383 tion steps. This industrializable process is thus promising for the preparation  
384 of thermoelectric materials and will be applied to more complex (multi-doped  
385 and -filled) skutterudites but also to other intermetallic thermoelectric materials  
386 such as clathrates, (half-)Heusler phases or transition metal silicides.

## 387 **Acknowledgements**

388 Francis Gouttefangeas is acknowledged for SEM images and EDS analyses per-  
389 formed on the CMEBA platform. TEM experiments were performed on THEMIS  
390 platform. Both platforms belong to the ScanMAT unit (UMS 2001, University of  
391 Rennes 1) which received a financial support from the European Union (CPER-  
392 FEDER 2007-2014).// Laura Paradis-Fortin is acknowledged for her careful  
393 reading of the article and correction of language errors.

- 394 [1] L. Yang, Z.-G. Chen, M. S. Dargusch, J. Zou, High Performance Thermo-  
395 electric Materials: Progress and Their Applications, *Adv. Energy Mater.* 8  
396 (2018) 1701797.
- 397 [2] B. C. Sales, D. Mandrus, R. K. Williams, Filled skutterudite antimonides:  
398 A new class of thermoelectric materials, *Science* 272 (1996) 1325–1328.
- 399 [3] G. S. Nolas, D. T. Morelli, T. M. Tritt, Skutterudites: A phonon-glass-  
400 electron crystal approach to advanced thermoelectric energy conversion  
401 applications, *Annu. Rev. Mater. Sci.* 29 (1999) 89–116.
- 402 [4] S. LeBlanc, S. K. Yee, M. L. Scullin, C. Dames, K. E. Goodson, Material  
403 and manufacturing cost considerations for thermoelectrics, *Renew. Sust.*  
404 *Energ. Rev.* 84 (2014) 313–327.
- 405 [5] G. Rogl, P. Rogl, Skutterudites, a most promising group of thermoelectric  
406 materials, *Curr. Opin. Green Sustainable Chem.* 4 (2017) 50–57.
- 407 [6] M. Puyet, C. Candolfi, L. Chaput, V. D. Ros, A. Dauscher, B. Lenoir, J. Hejt-  
408 manek, Low-temperature thermal properties of n-type partially filled cal-  
409 cium skutterudites, *J. Phys.:Condens. Matter* 18 (2006) 11301–11308.

- 410 [7] G. S. Nolas, J. Yang, H. Takizawa, Transport properties of germanium-  
411 filled  $\text{CoSb}_3$ , *Appl. Phys. Lett.* 84 (2004) 5210–5212.
- 412 [8] X. Y. Zhao, X. Shi, L. D. Chen, W. Q. Zhang, W. B. Zhang, Y. Z. Pei, Syn-  
413 thesis and thermoelectric properties of Sr-filled skutterudite  $\text{Sr}_y\text{Co}_4\text{Sb}_{12}$ ,  
414 *J. Appl. Phys.* 99 (2006) 053711.
- 415 [9] G. Rogl, A. Grytsiv, K. Yubuta, S. Puchegger, E. Bauer, C. Raju, R. C.  
416 Mallik, P. Rogl, In-doped multifolded n-type skutterudites with  $\text{ZT}=1.8$ ,  
417 *Acta Mater.* 95 (2015) 201–211.
- 418 [10] J. Gainza, F. Serrano-Sánchez, J. Prado-Gonjal, N. M. Nemes, N. Biskup,  
419 O. J. Dura, J. L. Martínez, F. Fauth, J. A. Alonso, Substantial thermal con-  
420 ductivity reduction in mischmetal skutterudites  $\text{Mm}_x\text{Co}_4\text{Sb}_{12}$  prepared un-  
421 der high-pressure conditions, due to uneven distribution of the rare-earth  
422 elements, *J. Mater. Chem. C* 7 (2019) 4124–4131.
- 423 [11] K. Wojciechowski, J. Tobola, J. Leszczynski, Thermoelectric properties and  
424 electronic structure of  $\text{CoSb}_3$  doped with Se and Te, *J. Alloys Compd.* 361  
425 (2003) 19–27.
- 426 [12] J. Mi, X. Zhao, T. Zhu, J. Ma, Thermoelectric properties of skutterudites  
427  $\text{Fe}_x\text{Ni}_y\text{Co}_{1-x-y}\text{Sb}_3$  ( $x=y$ ), *J. Alloys Compd.* 452 (2008) 225–229.
- 428 [13] Y. Lan, A. J. Minnich, G. Chen, Z. Ren, Enhancement of Thermoelectric  
429 Figure-of-Merit by a Bulk Nanostructuring Approach, *Adv. Funct. Mater.*  
430 20 (2010) 357–376.
- 431 [14] X. Meng, Z. Liu, B. Cui, D. Qin, H. Geng, W. Cai, L. Fu, J. He, Z. Ren, J. Sui,  
432 Grain Boundary Engineering for Achieving High Thermoelectric Perfor-  
433 mance in n-Type Skutterudites, *Adv. Energy Mater.* 7 (2017) 1602582.
- 434 [15] G. Joshi, H. Lee, Y. Lan, X. Wang, G. Zhu, D. Wang, R. W. Gould, D. C. Cuff,  
435 M. Y. Tang, M. S. Dresselhaus, G. Chen, Z. Ren, Enhanced Thermoelectric  
436 Figure-of-Merit in Nanostructured p-type Silicon Germanium Bulk Alloys,  
437 *Nano Lett.* 8 (2008) 4670–4674.

- 438 [16] L. Yang, Z. G. Chen, M. Hong, G. Han, J. Zou, Enhanced Thermoelectric  
439 Performance of Nanostructured  $\text{Bi}_2\text{Te}_3$  through Significant Phonon Scatter-  
440 ing, *ACS Appl. Mater. Interfaces* 7 (2015) 23694–23699.
- 441 [17] C. Recknagel, N. Reinfried, P. Höhn, W. Schnelle, H. Rosner, Y. Grin,  
442 A. Leithe-Jasper, Application of spark plasma sintering to the fabrication of  
443 binary and ternary skutterudites, *Sci. Tech. Adv. Mater.* 8 (2007) 357–363.
- 444 [18] V. Trivedi, M. Battabyal, P. Balasubramanian, G. M. Muralikrishna, P. K.  
445 Jain, R. Gopalan, Microstructure and doping effect on the enhancement  
446 of the thermoelectric properties of Ni doped Dy filled  $\text{CoSb}_3$  skutterudites,  
447 *Sustain. Energ. Fuels* 2 (2018) 2687–2697.
- 448 [19] G. Rogl, A. Grytsiv, R. Anbalagan, J. Bursik, M. Kerber, E. Schafler, M. Ze-  
449 hetbauer, E. Bauer, P. Rogl, Direct SPD-processing to achieve high-ZT skut-  
450 terudites, *Acta Mater.* 159 (2018) 352–363.
- 451 [20] L. Guo, G. Wang, K. Peng, Y. Yan, X. Tang, M. Zeng, J. Dai, G. Wangand,  
452 X. Zhou, Melt spinning synthesis of p-type skutterudites: Drastically speed  
453 up the process of high performance thermoelectrics, *Scripta Mater.* 116  
454 (2016) 26–30.
- 455 [21] S. Lee, K. H. Lee, Y.-M. Kim, H. S. Kim, G. J. Snyder, S. Baik, S. W. Kim,  
456 Simple and efficient synthesis of nanograin structured single phase filled  
457 skutterudite for high thermoelectric performance, *Acta. Mater.* 142 (2018)  
458 8–17.
- 459 [22] E. Godlewska, K. Mars, K. Zawadzka, Alternative route for the preparation  
460 of  $\text{CoSb}_3$  and  $\text{Mg}_2\text{Si}$  derivatives, *J. Solid State Chem.* 193 (2012) 109–113.
- 461 [23] F. Gucci, T. G. Saunders, M. J. Reece, In-situ synthesis of n-type un-  
462 filled skutterudite with reduced thermal conductivity by hybrid flash-spark  
463 plasma sintering, *Scripta Mater.* 157 (2018) 58–61.
- 464 [24] L. Kong, X. Jia, Y. Zhang, B. Sun, B. Liu, H. Liu, C. Wang, B. Liu, J. Chen,  
465 H. Ma, N-type  $\text{Ba}_{0.3}\text{Ni}_{0.15}\text{Co}_{3.85}\text{Sb}_{12}$  skutterudite: High pressure processing

- 466 technique and thermoelectric properties, *J. Alloys Compd.* 734 (2018) 36–  
467 42.
- 468 [25] L. Deng, J. Ni, L. Wang, X. Jia, J. Qin, B. Liu, Structure and thermoelectric  
469 properties of  $\text{In}_x\text{Ba}_y\text{Co}_4\text{Sb}_{12}$  samples prepared by HPHT, *J. Alloys Compd.*  
470 712 (2017) 477–481.
- 471 [26] A. Sesselmann, G. Skomedal, H. Middleton, E. Müller, The Influence of  
472 Synthesis Procedure on the Microstructure and Thermoelectric Proper-  
473 ties of p-Type Skutterudite  $\text{Ce}_{0.6}\text{Fe}_2\text{Co}_2\text{Sb}_{12}$ , *J. Electron. Mater.* 45 (2015)  
474 1397–1407.
- 475 [27] M. S. Toprak, C. Stiewe, D. Platzek, S. Williams, L. Bertini, E. Müller,  
476 C. Gatti, Y. Zang, M. Rowe, M. Muhammed, The impact of nanostruc-  
477 turing on the thermal conductivity of thermoelectric  $\text{CoSb}_3$ , *Adv. Funct.*  
478 *Mater.* 14 (2004) 1189–1196.
- 479 [28] Y. Li, C. Li, B. Wang, W. Li, P. Che, A comparative study on the thermo-  
480 electric properties of  $\text{CoSb}_3$  prepared by hydrothermal and solvothermal  
481 route, *J. Alloys Compd.* 772 (2019) 770–774.
- 482 [29] K. Biswas, J. He, I. D. Blum, C.-I. Wu, T. P. Hogan, D. N. Seidman, V. P.  
483 Dravid, M. G. Kanatzidis, High-performance bulk thermoelectrics with all-  
484 scale hierarchical architectures, *Nature* 489 (2012) 414–418.
- 485 [30] X. Meng, Z. Liu, B. Cui, D. Gin, H. Geng, W. Cai, L. Fu, J. He, Z. Ren,  
486 J. Sui, Grain Boundary Engineering for Achieving High Thermoelectric Per-  
487 formance in n-Type Skutterudite, *Adv. Energy Mater.* 7 (2017) 642–651.
- 488 [31] W. Li, J. Wang, Y. Xie, J. L. Gray, J. J. Heremans, H. B. Kang, B. Poudel,  
489 S. T. Huxtable, S. Priya, Enhanced thermoelectric performance of Yb-  
490 single-filled skutterudite by ultralow thermal conductivity, *Chem. Mater.*  
491 31 (2019) 862–872.



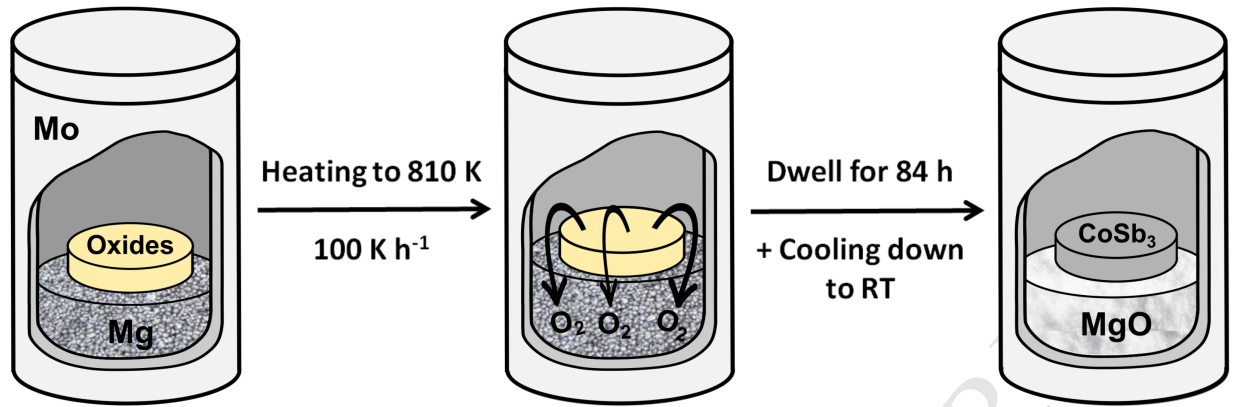
- 492 [32] G. Rogl, A. Grytsiv, P. Rogl, E. Bauer, M. B. Kerber, M. Zehetbauer,  
493 S. Puchegger, Multifilled nanocrystalline p-type didymium-Skutterudites  
494 with  $ZT > 1.2$ , *Intermetallics* 18 (2010) 2435–2444.
- 495 [33] M. Matsubara, Y. Masuoka, R. Asahi, Effects of doping IIIB elements (Al,  
496 Ga, In) on thermoelectric properties of nanostructured n-type filled skutterudite  
497 compounds, *J. Alloys Compd.* 774 (2019) 731–738.
- 498 [34] H. Yang, P. Wen, X. Zhou, Y. Li, B. Duan, P. Zhai, Q. Zhang, Enhanced ther-  
499 moelectric performance of Te-doped skutterudite with nano-micro-porous  
500 architecture, *Scripta Mater.* 159 (2018) 68–71.
- 501 [35] A. U. Khan, K. Kobayashi, D.-M. Tang, Y. Yamauchi, K. Hasegawa, M. Mit-  
502 ome, Y. Xue, B. Jiang, K. Tsuchiya, D. Golberg, Y. Bando, T. Mori, Nano-  
503 micro-porous skutterudites with 100% enhancement in ZT for high per-  
504 formance thermoelectricity, *Nano Energy* 31 (2017) 152–159.
- 505 [36] H. Li, X. Su, X. Tang, Q. Zhang, C. Uher, G. J. Snyder, U. Aydemir,  
506 Grain boundary engineering with nano-scale InSb producing highper-  
507 formance  $\text{In}_x\text{Ce}_y\text{Co}_4\text{Sb}_{12+z}$  skutterudite thermoelectrics, *J. Materiomics* 3  
508 (2017) 273–279.
- 509 [37] P. Chen, Z. Zhou, W. Jiang, Wei Luo, J. Yang, J. Zhu, L. Wang, Y. Fan, En-  
510 hancing the thermoelectric performance of filled skutterudite nanocom-  
511 posites in a wide temperature range via electroless silver plating, *Scripta*  
512 *Mater.* 146 (2018) 136–141.
- 513 [38] H. Zhao, B. Cao, S. Li, N. Liu, J. Shen, S. Li, J. Jian, L. Gu, Y. Pei, G. J.  
514 Snyder, Z. Ren, X. Chen, Engineering the Thermoelectric Transport in Half-  
515 Heusler Materials through a Bottom-Up Nanostructure Synthesis, *Adv. En-*  
516 *ergy Mater.* 7 (2017) 1700446.
- 517 [39] L. Ma, C. Y. Seo, X. Chen, K. Sun, J. W. Schwank, Indium-doped  $\text{Co}_3\text{O}_4$   
518 nanorods for catalytic oxidation of CO and  $\text{C}_3\text{H}_6$  towards diesel exhaust,  
519 *Appl. Catal. B-Environ.* 222 (2018) 44–58.

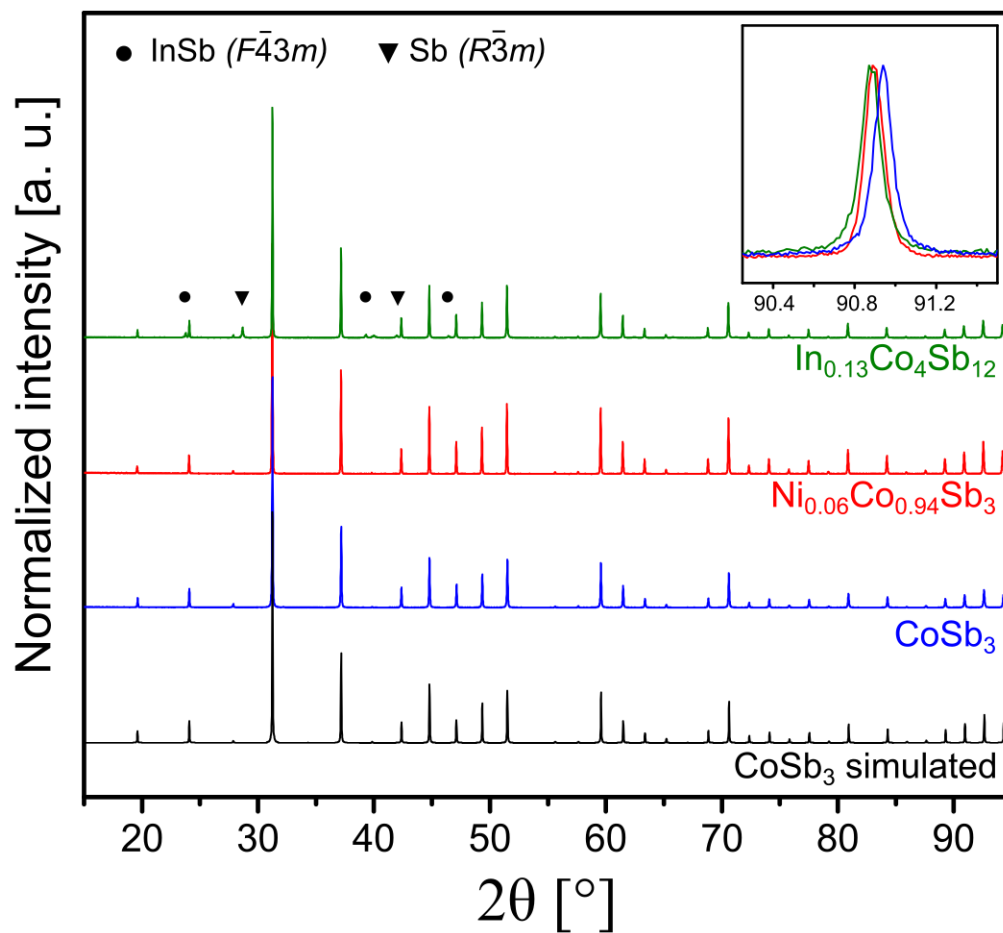
- 520 [40] E. Alleno, E. Zehani, O. Rouleau, Metallurgical and thermoelectric prop-  
521 erties in  $\text{Co}_{1-x}\text{Pd}_x\text{Sb}_3$  and  $\text{Co}_{1-x}\text{Ni}_x\text{Sb}_3$  revisited, *J. Alloys Compd.* 572  
522 (2013) 43–48.
- 523 [41] E. Alleno, E. Zehani, M. Gaborit, V. Orodniichuk, B. Lenoir, M. Benyahia,  
524 Mesostructured thermoelectric  $\text{Co}_{1-y}\text{M}_y\text{Sb}_3$  (M = Ni, Pd) skutterudites, *J.*  
525 *Alloys Compd.* 692 (2017) 676–686.
- 526 [42] T. He, J. Chen, H. D. Rosenfeld, M. A. Subramanian, Thermoelectric prop-  
527 erties of indium-filled skutterudites, *Chem. Mater.* 18 (2006) 759–762.
- 528 [43] R. C. . Mallik, J. Y. Jung, S. C. Ur, I. H. Kim, Thermoelectric properties of  
529  $\text{In}_z\text{Co}_4\text{Sb}_{12}$  skutterudites, *Met. Mater. Int.* 14 (2008) 223–228.
- 530 [44] J. Leszczynski, V. D. Ros, B. Lenoir, A. Dauscher, C. Candolfi, P. Mass-  
531 chelein, J. Hejtmanek, K. Kutorasinski, J. Tobola, R. I. Smith, C. Stiewe,  
532 E. Müller, Electronic band structure, magnetic, transport and thermody-  
533 namic properties of In-filled skutterudites  $\text{In}_x\text{Co}_4\text{Sb}_{12}$ , *J. Phys. D: Appl.*  
534 *Phys.* 46 (2013) 495106.
- 535 [45] R. C. Mallik, C. Stiewe, G. Karpinski, R. Hassdorf, E. Müller, Thermoelec-  
536 tric properties of  $\text{Co}_4\text{Sb}_{12}$  skutterudite materials with partial In filling and  
537 excess In additions, *J. Electron. Mater.* 38 (2009) 1337–1339.
- 538 [46] G. Li, K. Kurosaki, Y. Ohishi, H. Muta, S. Yamanaka, Thermoelectric prop-  
539 erties on Indium-added skutterudites  $\text{In}_x\text{Co}_4\text{Sb}_{12}$ , *J. Electron. Mater.* 42  
540 (2013) 1463–1468.
- 541 [47] E. Visnow, C. P. Heinrich, A. S. and J. de Boor, P. Leidich, B. Klobes, R. P.  
542 Hermann, W. E. Müller, W. Tremel, On the true Indium content on In-filled  
543 skutterudites, *Inorg. Chem.* 54 (2015) 7818–7827.
- 544 [48] J. Rodriguez-Carvajal, Recent advances in magnetic-structure determina-  
545 tion by neutron powder diffraction, *Physica B* 192 (1993) 55–69.

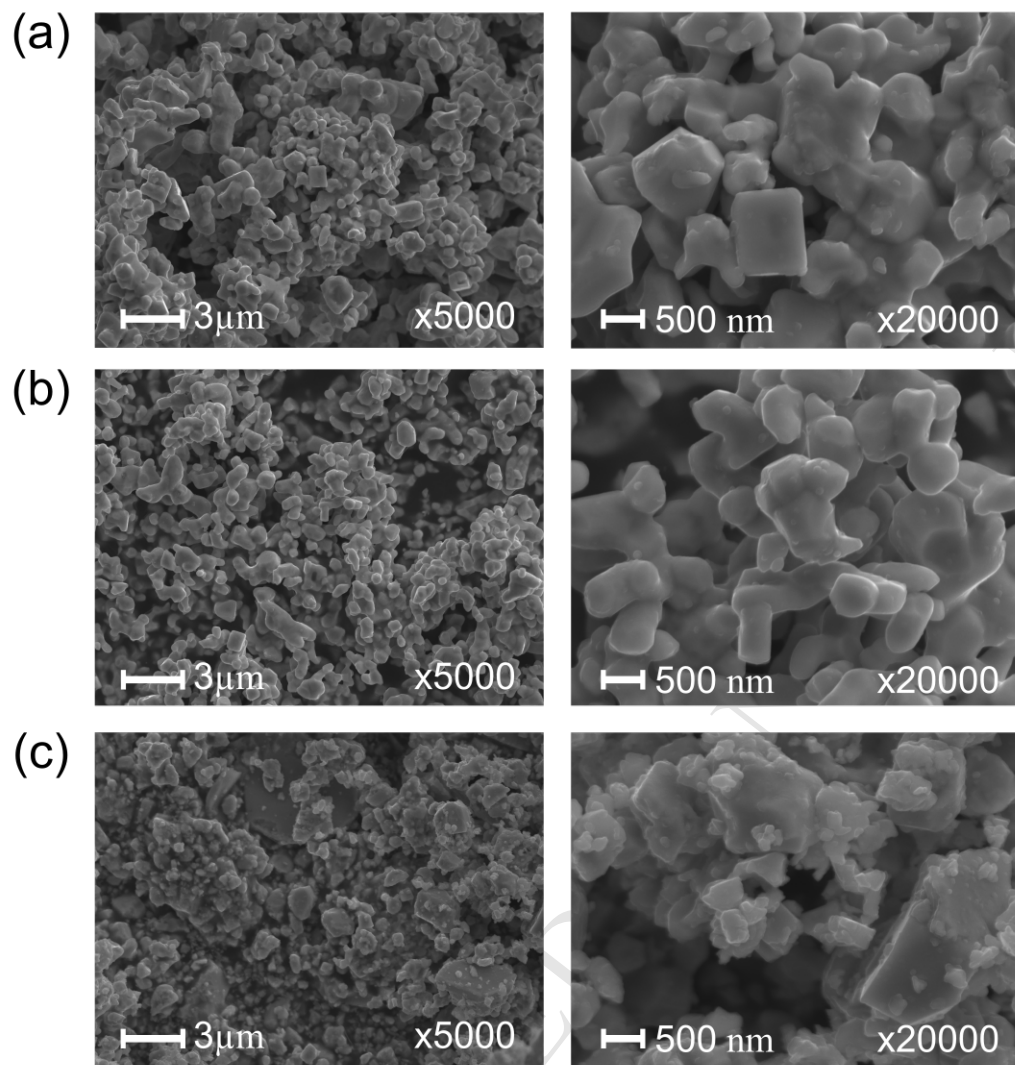
- 546 [49] O. Rouleau, E. Alleno, Measurement system of the Seebeck coefficient or of  
547 the electrical resistivity at high temperature, *Rev. Sci. Instrum.* 84 (2013)  
548 105103.
- 549 [50] D. G. Mandrus, A. Migliori, T. W. Darling, M. F. Hundley, E. J. Peterson,  
550 J. D. Thompson, Electronic transport in lightly doped  $\text{CoSb}_3$ , *Phys. Rev. B*  
551 52 (1995) 4926–4931.
- 552 [51] M. Christensen, B. B. Iversen, L. Bertini, C. Gatti, M. Toprak,  
553 M. Muhammed, E. Nishibori, Structural study of Fe doped and Ni substi-  
554 tuted thermoelectric skutterudites by combined synchrotron and neutron  
555 powder diffraction and *ab initio* theory, *J. Appl. Phys.* 96 (2004) 3148–  
556 3157.
- 557 [52] W. Zhao, P. Wei, Q. J. Zhang, H. Peng, W. T. Zhu, D. G. Tang, J. Yu,  
558 H. Y. Zhou, Z. Y. Liu, X. Mu, D. Q. He, J. C. Li, C. L. Wang, X. F. Tang,  
559 J. H. Yang, Multi-localization transport behaviour in bulk thermoelectric  
560 materials, *Nat. Commun.* 6 (2015) 6197.
- 561 [53] A. Grytsiv, P. Rogl, H. Michor, E. Bauer, G. Giester,  $\text{In}_y\text{Co}_4\text{Sb}_{12}$  Skutteru-  
562 dite: Phase Equilibria and Crystal Structure, *J. Electron. Mater.* 42 (2013)  
563 2940–2952.
- 564 [54] G. Champion, J. Allenou, M. Pasturel, H. Noël, F. Charollais, M. Anselmet,  
565 X. Iltis, O. Tougait, Magnesiothermic Reduction Process Applied to the  
566 Powder Production of U(Mo) Fissile Particles, *Adv. Eng. Mater.* 15 (2013)  
567 257–261.
- 568 [55] K. Choi, H. Choi, H. Na, I. Sohn, Effect of magnesium on the phase equi-  
569 libria in magnesio-thermic reduction of  $\text{Nb}_2\text{O}_5$ , *Mater. Lett.* 183 (2016)  
570 151–155.
- 571 [56] C. Won, H. Nersisyan, H. Won, Titanium powder prepared by a rapid  
572 exothermic reaction, *Chem. Eng. J.* 157 (2010) 270–275.

- 573 [57] H. J. T. Ellingham, Reducibility of oxides and sulfides in metallurgical  
574 processes, *J. Soc. Chem. Ind.* 63 (1944) 125–160.
- 575 [58] R. C. Sharma, T. L. Ngai, Y. A. Chang, The In-Sb (Indium-Antimony) sys-  
576 tem, *Bull. Alloy Phase Diagrams* 10 (1989) 657–664.
- 577 [59] G. Rogl, A. Grytsiv, P. Rogl, E. Royanian, E. Bauer, J. Horky, D. Setman,  
578 E. Schafner, M. Zehetbauer, Dependence of thermoelectric behaviour on  
579 severe plastic deformation parameters: A case study on p-type skutteru-  
580 dite  $\text{DD}_{0.60}\text{Fe}_3\text{CoSb}_{12}$ , *Acta. Mater.* 61 (2013) 6778–6789.
- 581 [60] L. Yang, J. Wu, L. Zhang, Synthesis of filled skutterudite compound  
582  $\text{La}_{0.75}\text{Fe}_3\text{CoSb}_{12}$  by spark plasma sintering and effect of porosity on ther-  
583 moelectric properties, *J. Alloys Compd.* 364 (2004) 83–88.
- 584 [61] J. Friedel, *Dislocations*, 1st Edition, Pergamon Press, 1964 (1964).
- 585 [62] Y. Kawaharada, K. Kurosaki, M. Uno, S. Yamanaka, Thermoelectric prop-  
586 erties of  $\text{CoSb}_3$ , *J. Alloys Compd.* 315 (2001) 193–197.
- 587 [63] J. W. Sharp, E. C. Jones, R. K. Williams, P. M. Martin, B. C. Sales, Thermo-  
588 electric properties of  $\text{CoSb}_3$  and related alloys, *J. Appl. Phys.* 78 (1995)  
589 1013–1018.
- 590 [64] H. Kitagawa, M. Wakatsuki, H. Nagaoka, H. Noguchi, Y. Isoda,  
591 K. Hasezaki, Y. Noda, Temperature dependence of thermoelectric prop-  
592 erties of Ni-doped  $\text{CoSb}_3$ , *J. Phys. Chem. Solid.* 66 (2005) 1635–1639.
- 593 [65] A. Sesselmann, B. Klobes, T. Dasgupta, O. Gourdon, R. Hermann,  
594 E. Müller, Neutron diffraction and thermoelectric properties of in-  
595 dium filled  $\text{In}_x\text{Co}_4\text{Sb}_{12}$  ( $x=0.05, 0.2$ ) and indium cerium filled  
596  $\text{Ce}_{0.05}\text{In}_{0.1}\text{Co}_4\text{Sb}_{12}$  skutterudites, *Phys. Stat. Sol. A* 213 (2016) 766–773.
- 597 [66] E. Alleno, D. Berardan, C. Bly, C. Candolfi, R. Daou, R. Decourt,  
598 E. Guilmeau, S. Hebert, J. Hejtmanek, B. Lenoir, P. Masschelein,  
599 V. Ohorodnichuk, M. Pollet, S. Populoh, D. Ravot, O. Rouleau, M. Soulier,

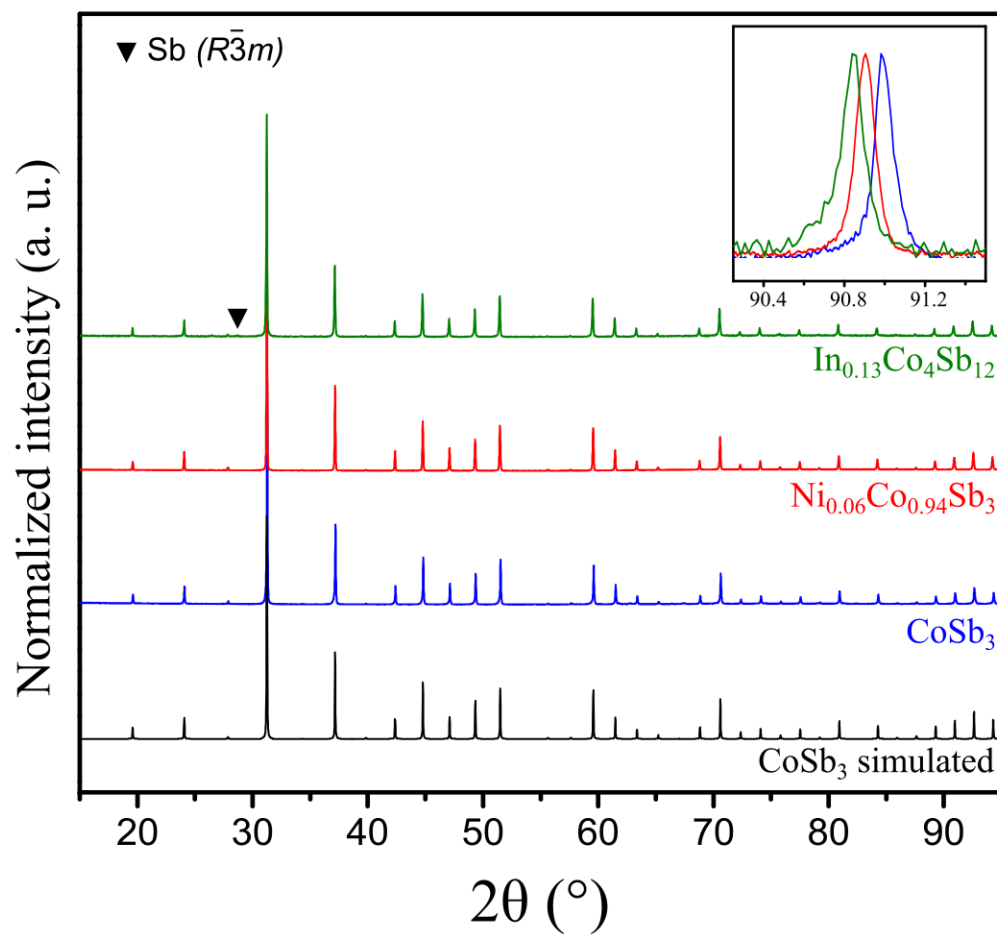
- 600 A round robin test of the uncertainty on the measurement of the thermo-  
601 electric dimensionless figure of merit of  $\text{Co}_{0.97}\text{Ni}_{0.03}\text{Sb}_3$ , *Rev. Sci. Instrum.*  
602 86 (2015) 011301.
- 603 [67] E. Alleno, L. Chen, Chubilleau, B. Lenoir, O. Rouleau, M. Trichet,  
604 B. Villeroy, Thermal Conductivity Reduction in  $\text{CoSb}_3$ - $\text{CeO}_2$  Nanocompos-  
605 ites, *J. Electron. Mater.* 39 (2010) 1966–1970.
- 606 [68] A. Khan, M. Saleemi, M. Johnsson, L. Han, N. Nong, M. Muhammed,  
607 M. Toprak, Fabrication, spark plasma consolidation, and thermoelectric  
608 evaluation of nanostructured  $\text{CoSb}_3$ , *J. Alloys Compd.* 612 (2014) 293–  
609 300.
- 610 [69] Q. He, Q. Hao, X. Wang, J. Yang, Y. Lan, X. Yan, B. Yu, Y. Ma, B. Poude,  
611 G. Joshi, D. Wang, G. Chen, Z. Ren, Nanostructured Thermoelectric Skut-  
612 terudite  $\text{Co}_{1-x}\text{Ni}_x\text{Sb}_3$  Alloys, *J. Nanosci. Nanotechnol.* 8 (2008) 4003–  
613 4006.
- 614 [70] M. Benyahia, V. Ohorodniichuk, E. Leroy, A. Dauscher, B. Lenoir, E. Alleno,  
615 High thermoelectric figure of merit in mesostructured  $\text{In}_{0.25}\text{Co}_4\text{Sb}_{12}$  n-type  
616 skutterudite, *J. Alloys Compd.* 735 (2018) 1096–1104.
- 617 [71] C. W. Nan, R. Birringer, Determining the Kapitza resistance and the ther-  
618 mal conductivity of polycrystals: A simple model, *Phys. Rev. B* 14 (1998)  
619 8264–8268.
- 620 [72] H. S. Yang, G. Bai, L. Thompson, J. Eastman, Interfacial thermal resistance  
621 in nanocrystalline yttria-stabilized zirconia, *Acta Mater.* 50 (2002) 2309–  
622 2317.
- 623 [73] G. A. Slack, Design Concepts for Improved Thermoelectric Materials, *MRS*  
624 *Proceedings* 478 (1997) 47.

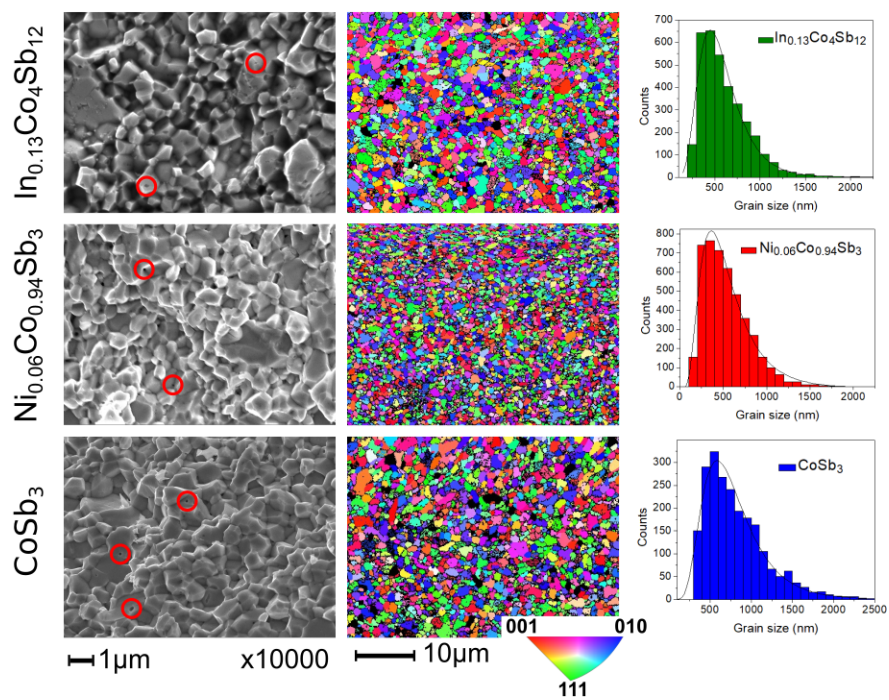


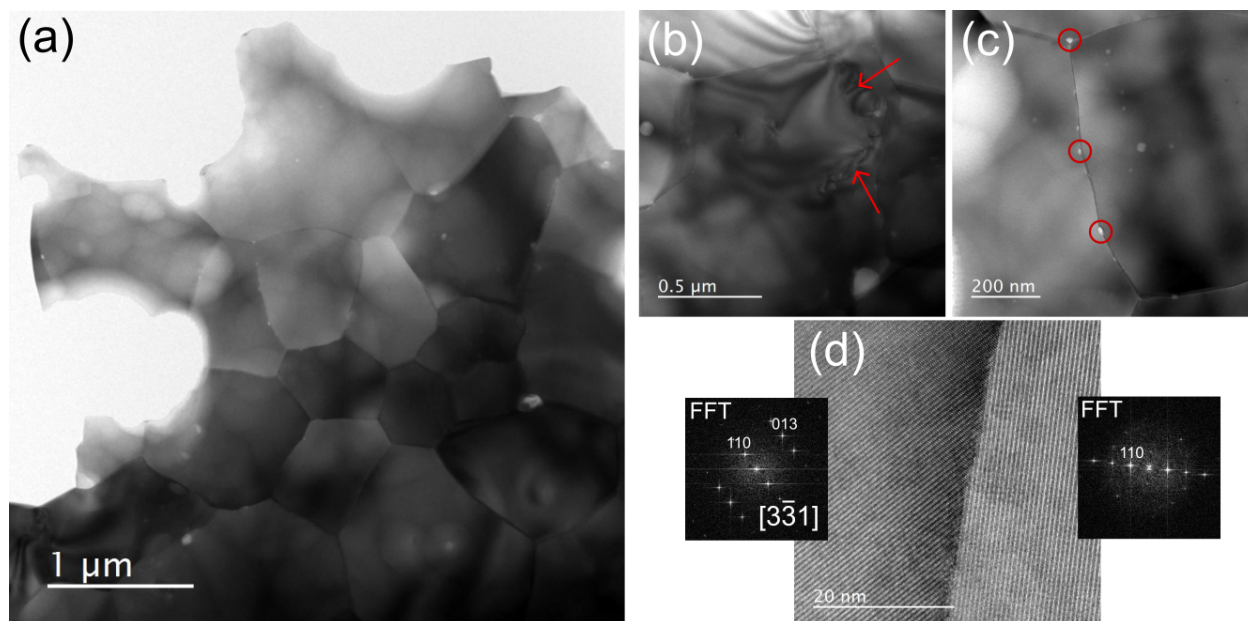




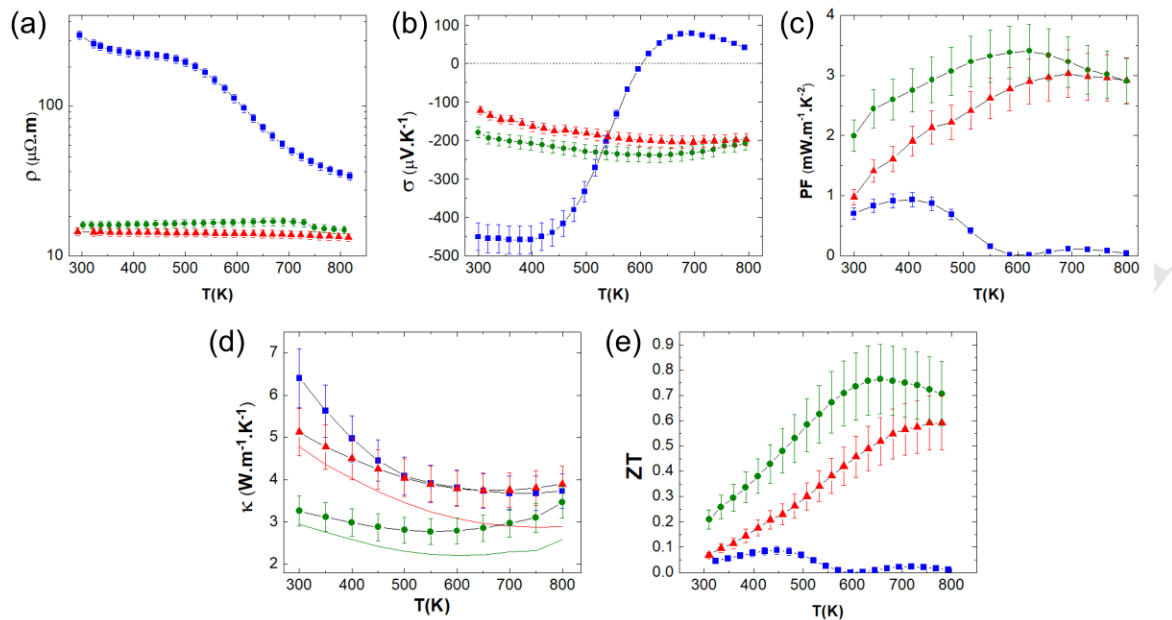








ACCEPTED MANUSCRIPT



- Magnesio-reduction of oxides is used to prepare skutterudites.
- Well-crystallized and submicronic powders are obtained at low temperature.
- The mesostructure survives after spark plasma sintering.
- Accordingly, improved thermoelectric performances are achieved.
- Thermoelectric properties are discussed toward microstructure of the materials.

ACCEPTED MANUSCRIPT